SAND2013-10471C

Non-equilibrium gas-liquid interface dynamics in high-pressure liquid injection systems

Rainer N. Dahms and Joseph C. Oefelein

Combustion Research Facility, Sandia National Laboratories, Livermore, CA 94551, USA

Corresponding author:
Rainer N. Dahms
Sandia National Laboratories, Combustion Research Facility
7011 East Avenue, MS9051
Livermore, CA 94550
Email: Rndahms@sandia.gov

- Colloquium topic: Spray and Droplet Combustion
- Keywords: Liquid injection; Diesel engine; Cahn-Hilliard equation; Real fluid model; Non-equilibrium thermodynamics
- Short running title: Non-equilibrium gas-liquid interface dynamics in high-pressure liquid injections
- Word count:
  1. Abstract: 296 words (word processor)
  2. Equations: 276 words (using formula)
  3. Figures: 1640 words (using formula)
  4. References: 857 words (using formula)
  5. Number of words: 3022 words (word processor)

  Paper length: 5795 words (method 1)
- The authors agree to pay color reproduction charges

Submitted for Consideration of Publication in the Proceedings of the Combustion Institute

Thirty-Fifth International Symposium on Combustion
San Francisco, USA
August 3 – 8, 2014.

Abstract

The transition of classical spray atomization processes to single-phase continuous dense-fluid mixing dynamics is poorly understood. Recently, a theory has been presented that established, based on a Knudsen-number criterion, that the development of such mixing layers is initiated because the multicomponent two-phase interface becomes much wider than the mean free molecular path. This shows that the transition to mixing layers occurs due to interfacial dynamics and not, as conventional wisdom had suggested, because the liquid phase has heated up to supercritical temperatures where surface tension forces diminish. In this paper we focus on the dynamics of this transition process, which still poses many fundamental questions. We show that such dynamics are dictated by substantial statistical fluctuations and the presence of significant interfacial free energy forces. The comprehensive analysis is performed based on a combination of non-equilibrium mean-field thermodynamics and a detailed modified 32-term Benedict-Webb-Rubin mixture state equation. Statistical fluctuations are quantified using the generally accepted model of Poisson-distributions for variances systems with a small number of molecules. Such fluctuations quantify the range of pressure and temperature conditions under which the gradual transition to dense-fluid mixing dynamics occurs. The interface begins to deteriorate as it broadens substantially, and the related interfacial free energy forces do not instantly diminish only because vapor-liquid equilibrium conditions do not apply anymore. Instead, such forces are shown to gradually decrease and to diminish once the interface enters the continuum regime. At this point the interfacial region becomes a continuous gas-liquid mixing layer that is significantly affected by single-phase real-fluid thermodynamics and transport properties.

Keywords: Direct injection; Diesel engine; Supercritical flow; Real fluid model; Nonequi-

librium thermodynamics.

1 Introduction

Mayer *et al.* [1,2] were one of the first to show that under certain high-pressure conditions, the presence of the widely recognized spray atomization and evaporation process is replaced by diffusion-dominated dense-fluid mixing layers. Past research into multiphase flows has provided additional insights into the physics of high-pressure fluid dynamics [3–19]. Despite these prior contributions, modern theory has lacked a first principle explanation for the observed phenomena. To address this, Dahms and Oefelein have recently presented such a theory that explains and quantifies the conditions under which a multicomponent mixture transitions from classical spray atomization processes to dense-fluid mixing [20, 21]. They developed a system of models which coupled real-fluid thermodynamics in multicomponent and multiphase mixtures with vapor-liquid equilibrium and Linear Gradient Theory. The vapor-liquid equilibrium calculations provided the compositions and mixture states of the respective vapor and liquid phases. Linear Gradient Theory provided the detailed spatial distribution of these compositions across the two-phase interfacial region.

Gradient Theory was established by van der Waals [22,23] in 1893 and reformulated later by Cahn and Hilliard [24] in 1958 to compute the physical and continuous variation of fluid properties across a thin molecular vapor-liquid interface. The capability of Gradient Theory to calculate the physical mean molecular structure across such interfaces has recently been confirmed by statistical analysis of molecular dynamic simulations [25–27]. The analysis showed that the enthalpy contained in hot unburnt ambient gases is usually not sufficient to heat up the multicomponent gas-liquid interface to its critical temperature where surface tension forces diminish. Instead, the theory indicated that the transition to dense-fluid mixing layers occurs through combination of broadening two-phase interfaces, reduction in mean free path, and a reduction in surface tension. The broadening of the interface was mainly attributed to high subcritical gas-liquid interface temperatures, while the reduction

of the mean free path was mainly attributed to high pressure. This showed, based on an interface Knudsen-number criterion, that at certain high pressure and temperature conditions, the multicomponent two-phase interface becomes much wider than the mean free molecular path. Then, the transition to dense-fluid mixing layers occurs as the interface substantially departs from classical molecular behavior.

In this paper, the formerly presented theory is extended to quantify the non-equilibrium dynamics of the transition process. The analysis shows that the initiation of this transition is determined by substantial statistical fluctuations. Such variations are shown to decrease with increasing pressure and temperature conditions. The resulting probability of departing from vapor-liquid equilibrium conditions quantifies the range of pressure and temperature conditions under which the gradual transition to dense-fluid mixing dynamics occurs. When this happens, the interface begins to broaden substantially. Non-equilibrium mean-field thermodynamics, based on the Cahn-Hilliard equation [24], in combination with a detailed mixture state equation, are adopted to calculate corresponding interfacial free energy forces. The analysis shows that these forces do not instantly diminish only because the two-phase interface departs from classical molecular behavior. Instead, such forces are shown to gradually decrease and vanish once the interface enters the continuum regime. To illustrate the framework, we focus on conditions typical of diesel engine injection. The analysis, however, is quite general and applies to a wide range of modern propulsion and power systems.

2 Model Formulation

The coupled system of models employed is based on the theoretical-numerical framework developed by Oefelein [28,29]. It provides a detailed mixture state equation for the evaluation of thermodynamic and transport processes in a hydrocarbon mixture. This framework is combined with non-equilibrium mean-field thermodynamics of two-phase interfaces. The formulation is based on the Cahn-Hilliard equation and is shown to converge to the equations of Gradient Theory in the limit of thermodynamic equilibrium.

2.1 Thermodynamic and Transport Properties

A modified 32-term Benedict-Webb-Rubin (BWR) equation of state is applied in conjunction with the extended corresponding states model and non-linear mixing rules to calculate the p-v-T behavior of multicomponent mixtures [30, 31]. This framework has been shown to provide accurate results over a wide range of pressures, temperatures and mixture states, especially at saturated liquid conditions. The thermodynamic properties of real-fluid mixtures are obtained in two steps. First, respective component properties are combined at a fixed temperature using the extended corresponding states methodology to obtain the mixture state at a given reference pressure. A pressure correction is then applied using departure functions of the form given by Reid *et al.* [32, Chapter 5]. These functions are exact relations derived using Maxwell's relations (see for example VanWylen and Sonntag [33, Chapter 10]) and make full use of the real mixture p-v-T path dependencies dictated by the equation of state. Standard state properties are obtained using the databases developed by Gordon and McBride [34] and Kee *et al.* [35]. Chemical potentials and fugacity coefficients are obtained in a similar manner. Likewise, viscosity and thermal conductivity are obtained using the extended corresponding states methodologies developed by Ely and Hanley [36,37]. Mass and thermal diffusion coefficients are obtained using

the methodologies outlined by Bird *et al.* [38] and Hirschfelder *et al.* [39] in conjunction with the corresponding states methodology of Takahashi [40].

2.2 Non-Equilibrium Mean-Field Thermodynamics for Gas-Liquid Interface Structures

The starting point of the model is the formulation of the Helmholtz free energy across a two-phase interface. Assuming a quasi one-dimensional composition change, the total energy F is governed by the following equation according to van der Waals [22, 23] and Cahn and Hilliard [24]:

$$F = \int \left[f_0(\varrho, T) + \kappa (\nabla \varrho)^2 \right] dx \tag{1}$$

with f_0 defined as the Helmholtz free energy density of a homogeneous fluid, ϱ as the density, and κ as the density-independent influence parameter which reflects the molecular interfacial structure [41]. The Helmholtz free energy density is defined as

$$f_0(\varrho, T) = \varrho \mu - p \tag{2}$$

with μ as the chemical potential and with p as the pressure. It is important to note that Eq. (1) carries no assumptions that would restrict its validity to equilibrium conditions. It therefore serves to introduce a generalized definition of interfacial free energy forces. According to Cahn and Hilliard [24], such forces are defined as the result of the difference of the physical Helmholtz free energy across the two-phase interface, modeled by Eq. (1), and its homogeneous distribution as it would exist if the interface were not be present. In combination with Eq. (1), the equation to calculate interfacial free energy forces for

non-equilibrium gas-liquid interfaces is then

$$\sigma = \int \left[f_0(\varrho, T) + \kappa (\nabla \varrho)^2 - X_r \mu_r - (1 - X_r)\mu \right] dx \tag{3}$$

with X_r as the mole fraction of the reference component [21]. In order to solve Eq. (3), the density-temperature profile across the interface has to be obtained. This requires modeling and a corresponding modeling approach is presented later. In the limit of thermodynamic equilibrium, however, no such modeling is required. Then, the species profile across the interface can be obtained according to Gradient Theory by minimizing the Helmholtz free energy as follows [42, 43]

$$\kappa (\nabla \varrho)^2 = \bar{\omega}(\varrho) - \bar{\omega}_s \tag{4}$$

Here $\bar{\omega}_s = -p_s$ is the equilibrium pressure. The grand thermodynamic potential energy density is defined as

$$\bar{\omega}(\varrho) = f_0(\varrho) - \sum_i \varrho_i \, \mu_i \tag{5}$$

Hence, the equilibrium interfacial free energy force, the surface tension, reads after transforming the spatial coordinates to density coordinates according to Gradient Theory [42,43]

$$\sigma_{eq} = \int_{\varrho_{r,V}}^{\varrho_{r,L}} \sqrt{2\kappa \left(\bar{\omega}(\varrho) - \bar{\omega}_s \right)} d\rho_r \tag{6}$$

Here, $\varrho_{r,V}$ and $\varrho_{r,L}$ refer to the vapor and liquid phase densities of the reference component obtained by real-fluid vapor-liquid equilibrium calculations. It is important to note that Eq. (3) leads to the same result as Eq. (6) if the same equilibrium density profile is applied.

3 Results and Discussion

To perform the analysis, we focus on conditions similar to the "Spray A" nonreactive case defined as a relevant diesel engine condition as part of the Sandia National Laboratories "Engine Combustion Network" (see www.sandia.gov/ECN) [44, 45]. N-dodecane is injected as a liquid at a temperature of $T_{C_{12}} = 363$ K into nitrogen at a temperature of $T_{N_2} = 900$ K and a chamber pressure of $p = 60$ bar.

Figure 1 presents the regime diagram of microscale flows according to Bird [46]. The diagram is based on the four characteristic length scales of representative molecule size d, mean molecular spacing δ, mean free path λ, and characteristic length scale L and contains three different regime separators. The first is represented by L/δ=100 as the number of molecules within a volume element at which statistical fluctuations about the average molecule number N diminish. Only then, the continuum approximation applies. Present statistical fluctuations are quantified using the generally accepted model of a Poisson-distribution [46]

$$P(N) = (nV)^N \exp(-nV)/N! \tag{7}$$

with n as the average molecule number per unit volume and with V as the system volume. These quantities are related to the mean molecular spacing $n=\delta^{-3}$ and to the characteristic length scale $V=L^3$, respectively. The second regime separator is represented by the Knudsen number $Kn=\lambda/L=0.1$ at which the shear stresses, heat fluxes, and diffusion velocities become linear functions of the gradients in velocity, temperature, and species concentration within the validity of the classical kinetic Chapman-Enskog theory. The Knudsen number

is related to the former regime separator L/δ as follows

$$\mathrm{Kn} = \lambda/L \sim \frac{\delta}{L}\left(\frac{\delta}{d}\right)^2 \tag{8}$$

According to this relationship, the continuum approximation is always fulfilled at Knudsen numbers smaller than Kn=0.1 at high normalized molecular distances δ/d. At a particular distance, however, this relationship reverses. This condition defines the third regime separator as $\delta/\mathrm{d} \approx 7$ as the distinction between dilute gases and dense fluids. These definitions also establish the regime where the Navier-Stokes equations are valid.

Figure 1 also shows the location of low-pressure and high-pressure gas-liquid interfaces within the regime diagram. The characteristic length scale L is chosen to be the thickness of the interface. The molecular size d is the species molar fraction averaged diameter of a mixture conditioned on the vapor equilibrium composition [21]. The corresponding detailed interfacial density structures are shown as inset plots in the regime diagram and present results from former studies [20, 21]. Both interfaces are located in the molecular chaos regime. Therefore, their interfacial dynamics are dictated by substantial statistical fluctuations.

Figure 2 shows the PDF of the corresponding molecule numbers calculated from Eq. (7). The low-pressure interface has a lower value of the average molecule number (nV=10) and a higher coefficient of variation ($c_v \approx 0.32$) in comparison to the high-pressure interface (nV=27, $c_v \approx 0.19$). From these fluctuations, the corresponding variations in interface Knudsen-numbers can be derived. It is important to realize that the Knudsen-number of the high-pressure interface $\widetilde{\mathrm{Kn}} \approx 0.05$ is also subject to statistical fluctuations.

The regime diagram in Fig. 1 and Eq. (8) both illustrate that the association of the continuum regime, where such fluctuations are negligible, with Knudsen-numbers $\mathrm{Kn} < 0.1$ is only valid in the dilute gas regime but not in the dense-fluid regime. It also illustrates

that the Navier-Stokes equations are not valid under these conditions. The relationship between the Knudsen-number and the molecule number is established by recasting Eq. (8) as follows

$$\mathrm{Kn} \sim \frac{\delta}{L}\left(\frac{\delta}{d}\right)^2 = \left(\frac{\delta}{L}\right)^3\left(\frac{L}{d}\right)^2 = \frac{1}{N}\left(\frac{L}{d}\right)^2 \tag{9}$$

with d being constant in a specified fuel-oxidizer mixture. The relationship between the interface thickness L and the molecule number N is established by Gradient Theory.

In Gradient Theory, surface tension forces and interfacial thicknesses are calculated based on Eq. (4). When the density gradient term $\nabla\varrho$ is replaced by $\nabla\varrho = \varrho/\mathrm{L}$, the statistical fluctuations of the interface thickness L can be related to fluctuations in molecule numbers N on the assumption of a constant surface tension force. Molecular dynamic simulations such as those presented by Feller et al. support this assumption [47]. The density is related to the molecule number as $\varrho = m \cdot N/V$, with m as the mass of an individual molecule.

In combination with Eq. (9) the relationship between Knudsen-number and molecule number fluctuations reads as follows

$$\mathrm{Kn}'' \sim \mathrm{N}''^{13/9} \tag{10}$$

The corresponding PDF of the low-pressure and high-pressure interfacial Knudsen-numbers are shown in Fig. 3. The analysis illustrates that the probability of $\mathrm{Kn} > 0.1$ of the low-pressure interface is almost unity. This shows that this interface is governed by classical two-phase theory. However, the probability of the high-pressure interface to experience $\mathrm{Kn} < 0.1$ is $\mathrm{P}(\mathrm{Kn}<0.1) \approx 0.986$. Classical two-phase theory does not apply and this interface is governed by non-equilibrium thermodynamics and the presence of substantial interfacial

free energy forces.

In the following, the analysis focuses on the high-pressure interface only. The deviation of this interface from vapor-liquid equilibrium is illustrated in Fig. 4. It shows the envelope of vapor-liquid equilibrium mixture compositions for all possible temperatures at a pressure of p=60 bar. The adiabatic mixing temperature, defined in [20, 21], intersects the vapor equilibrium line at T≈545 K. This intersection establishes the representative vapor state at these injection conditions [20, 21]. The two-phase interface would manifest as a molecular isothermal interface if vapor-liquid equilibrium would apply. Under the conditions here, however, the interfacial region supports the development of thermal gradients ($\widetilde{\mathrm{Kn}} \approx 0.05 < 0.1$). The resulting temperature distribution is therefore assumed to obey the adiabatic mixing temperature distribution. The consequence of these different temperature variations on the interfacial density profile is shown in Fig. 5.

Figure 5 (top) shows the density profile using the molecular isothermal interface assumption according to Gradient Theory. Figure 5 (bottom) shows the density profile using the mixture fraction-temperature relationship provided by the adiabatic mixing line. Such a temperature distribution across the interface leads to an increased density gradient and an increased density in the compressed liquid phase. Once the interface distinctively departs from the equilibrium state, the interfacial region begins to deteriorate as it broadens substantially.

Figure 6 shows three different interfacial profiles representing various stages in the progress of this deterioration. During this process, the interfacial free energy forces are calculated using non-equilibrium thermodynamics according to Eq. (3). The density profile, shown in Fig. 5 (bottom), provides the modeling closure in order to solve Eq. (3) as discussed in Sec. 2.2. The analysis shows that such interfacial free energy forces do not instantly diminish only because vapor-liquid equilibrium conditions do not apply anymore.

Instead, such forces are shown to gradually decrease as the interface continues to broaden. Meanwhile, the mean interfacial Knudsen-number continues to decrease while the sample size increases substantially. This pathway of the interfacial region is also shown as the non-equilibrium path in the regime diagram in Fig. 1. With the gradual increase of the sample size, the effects of statistical fluctuations on the dynamics of the interfacial region vanish. Eventually, the interfacial region enters the continuum regime where the Navier-Stokes equations become valid ($\mathrm{Kn} < 0.1$; $\mathrm{L}/\delta > 100$). Then, the transport properties across the gas-liquid mixing layer can be calculated as outlined in Sec. 2.1.

Figure 7 (top) presents the diffusivities and Prandtl numbers as a function of the fuel mixture fraction at constant pressure p=60 bar and at a temperature distribution prescribed by the adiabatic mixing temperature shown in Fig. 4. Figure 7 (bottom) shows the species specific Schmidt numbers of nitrogen and dodecane. The analysis shows the transport non-idealities in the compressed liquid region. These are determined by high Schmidt and Prandtl numbers and by low diffusivities in comparison to the gaseous region. The diffusivities at ambient and liquid injection conditions read $\mathcal{D} \approx 6.86 \times 10^{-7}$ m^2/s and 2.51×10^{-8} m^2/s, respectively. The diffusivity of the compressed liquid phase is therefore more than an order of magnitude smaller than the ambient gas diffusivity.

4 Summary and Conclusions

Past research has suggested that injected liquid jets exhibit two distinctively different sets of evolutionary processes. At low pressure conditions, the classical situation exists where a well-defined two-phase interface along with its surface tension forces lead to the widely recognized spray atomization and evaporation processes. Under some high-pressure conditions, however, the presence of such discrete two-phase flow processes becomes diminished. Results of a recent research have suggested that the deterioration of the classical two-phase interface is initiated because its multicomponent structure becomes much wider than the mean free molecular path. Then, the gas-liquid interfacial region substantially departs from vapor-liquid equilibrium conditions which initiates the transition to dense-fluid mixing layers.

In order to analyze the dynamics of this transition process, a combination of non-equilibrium mean-field thermodynamics and a detailed mixture state theory was applied. The analysis shows that transition dynamics are governed by significant statistical fluctuations and the presence of distinct interfacial free energy forces. Statistical fluctuations in molecule numbers are shown to translate into variations of interfacial Knudsen-numbers under all relevant pressure and temperature conditions. This result illustrates that the association of the continuum regime, where statistical fluctuations are negligible and $\mathrm{Kn} < 0.1$, is only valid in the dilute gas regime but not in the dense-fluid regime associated with high-pressure liquid injection processes.

The statistical variation of interfacial Knudsen numbers were shown to decrease with increasing temperature and pressure of the ambient gas. The resulting probability of the interface to enter the $\mathrm{Kn} < 0.1$ regime is identified as a first principle mechanism to explain and quantify the range of pressure and temperature conditions under which the gradual transition to dense-fluid mixing dynamics takes place. Then, the two-phase interfacial

region begins to depart from classical isothermal behavior as prescribed by vapor-liquid equilibrium. Instead, the interfacial region supports the development of thermal gradients. Such gradients have been quantified and were shown to have a distinct influence on the interfacial density profile and its free energy forces.

In addition to the above, the analysis has also shown that interfacial forces do not instantly vanish. Instead, they gradually decrease as the interface deteriorates and diminish once the interface enters the continuum regime. Then, the developing dense-fluid mixing layer evolves under the presence of single-phase real-fluid thermodynamics and transport properties. Note that transport properties cannot be calculated accurately by classical real-fluid thermodynamics while the interface is transitioning due to the presence of substantial interfacial free energy forces and significant statistical fluctuations. Without proper and accurate transport properties, no conclusions can be obtained on the time scales of the transition process. Such time scales are imperative for the formulation of a modes that are capable of representing the related physical phenomena in continuum-based approaches. Understanding these time-history effects will be the subject of future research.

5 Acknowledgements

Support provided by the U. S. Department of Energy; Office of Science (SC), Basic Energy Sciences (BES) program under grant number KC0301020 is gratefully acknowledged. This research was performed at the Combustion Research Facility, Sandia National Laboratories, Livermore, California. Sandia National Laboratories is a multiprogram laboratory operated by Sandia Corporation, a Lockheed Martin Company, for the United States Department of Energy under contract DE-AC04-94-AL85000.

References

[1] W. Mayer, H. Tamura, *J. Prop. Power* 12 (6) (1996) 1137–1147.

[2] W. Mayer, A. Schik, B. Vieille, C. Chaveau, I. Gökalp, D. Talley, R. Woodward, *J. Prop. Power* 14 (5) (1998) 835–842.

[3] B. Chehroudi, *Intl. J. Aerospace Engineering* 2012 (2012) 1–31.

[4] M. Oschwald, J. Smith, R. Branam, J. Hussong, A. Schik, B. Chehroudi, D. Talley, *Combust. Sci. Tech.* 178 (1-3) (2006) 49–100.

[5] M. Habiballah, M. Orain, F. Grisch, L. Vingert, P. Gicquel, *Combust. Sci. Tech.* 178 (1-3) (2006) 101–128.

[6] R.N. Dahms, C. Felsch, O. Röhl, N. Peters, *Proc. Combust. Inst.* 33 (2011) 3023–3030.

[7] K.-C. Lin, S. Cox-Stouffer, T. Jackson, *Combust. Sci. Tech.* 178 (1-3) (2006) 129–160.

[8] S. Candel, M. Juniper, G. Singla, P. Scouflaire, C. Rolon, *Combust. Sci. Tech.* 178 (1-3) (2006) 161–192.

[9] R.N. Dahms, T.D. Fansler, M.C. Drake, T.-W. Kuo, A.M. Lippert, N. Peters, *Proc. Combust. Inst.* 32 (2009) 2743–2750.

[10] N. Zong, V. Yang, *Combust. Sci. Tech.* 178 (1-3) (2006) 193–228.

[11] J. C. Oefelein, *Combust. Sci. Tech.* 178 (1-3) (2006) 229–252.

[12] J. Bellan, *Combust. Sci. Tech.* 178 (1-3) (2006) 253–281.

[13] R.N. Dahms, M.C. Drake, T.D. Fansler, R.O. Grover, A.S. Solomon, *SAE Int. J. Engines* 5 (2012) 141–161.

[14] L. C. Selle, N. A. Okong'o, J. Bellan, K. G. Harstad, *J. Fluid Mech.* 593 (2007) 57–91.

[15] G. Ribert, N. Zong, V. Yang, L. Pons, N. Darabiha, S. Candel, *Combust. Flame* 154 (2008) 319–330.

[16] L. Pons, N. Darabiha, S. Candel, G. Ribert, V. Yang, *Combust. Theory Model.* 13 (2009) 57–81.

[17] T. Schmitt, Y. Méry, M. Boileau, S. Candel, *Proc. Combust. Inst.* 33 (2011) 1383–1390.

[18] R.N. Dahms, M.C. Drake, T.D. Fansler, T.-W. Kuo, N. Peters, *Combust. Flame* 158 (2011) 2229–2244.

[19] R.N. Dahms, M.C. Drake, T.D. Fansler, T.-W. Kuo, N. Peters, *Combust. Flame* 158 (2011) 2245–2260.

[20] R.N. Dahms, J. Manin, L.M. Pickett, J.C. Oefelein, *Proc. Combust. Inst.* 34 (2013) 1667–1675.

[21] R.N. Dahms, J.C. Oefelein, *Phys. Fluids* 25 (2013) 092103.

[22] J.D. van der Waals, *Verhandel Konik Akad Weten Amsterdam* 1 (1893) 8.

[23] J.S. Rowlinson, *J. Stat. Phys.* 20 (1979) 200–244.

[24] J.W. Cahn, J.E. Hilliard, *J. Chem. Phys.* 28 (2) (1958) 258–267.

[25] E.A. Müller, A. Mejia, *Fluid Phase Equil.* 282 (2009) 68–91.

[26] A. Mejia, J.C. Pamies, D. Duque, H. Seguara, L.F. Vega, *J. Chem. Phys.* 123 (2005) 1–10.

[27] C. Miqueu, J.M. Miguez, M.M. Pineiro, T. Lafitte, B. Mendiboure, *J. Phys. Chem. B* 115 (2011) 9618–9625.

[28] J. C. Oefelein, *Progress in Aerospace Sciences* 42 (1) (2006) 2–37.

[29] J. C. Oefelein, *Simulation and Analysis of Turbulent Multiphase Combustion Processes at High Pressures*, Ph.D. thesis, The Pennsylvania State University, University Park, Pennsylvania (May 1997).

[30] T. W. Leland, P. S. Chappelear, *Industrial and Engineering Chemistry Fundamentals* 60 (7) (1968) 15–43.

[31] J. S. Rowlinson, I. D. Watson, *Chem. Eng. Sci.* 24 (8) (1969) 1565–1574.

[32] R. C. Reid, J. M. Prausnitz, B. E. Polling, *The Properties of Liquids and Gases*, 4th Edition, McGraw-Hill, New York, New York, 1987.

[33] G. J. VanWylen, R. E. Sonntag, *Fundamentals of Classical Thermodynamics*, 3rd Edition, John Wiley and Sons, Incorporated, New York, New York, 1986.

[34] S. Gordon, B. J. McBride, *Computer Program for Calculation of Complex Chemical Equilibrium Compositions, Rocket Performance, Incident and Reflected Shocks and Chapman-Jouguet Detonations*, Tech. Rep. NASA SP-273, National Aeronautics and Space Administration (1971).

[35] R. J. Kee, F. M. Rupley, J. A. Miller, *Chemkin Thermodynamic Data Base*, Tech. Rep. SAND87-8215B, Sandia National Laboratories, supersedes SAND87-8215 dated April 1987 (1990).

[36] J. F. Ely, H. J. M. Hanley, *Industrial and Engineering Chemistry Fundamentals* 20 (4) (1981) 323–332.

[37] J. F. Ely, H. J. M. Hanley, *Industrial and Engineering Chemistry Fundamentals* 22 (1) (1981) 90–97.

[38] R. B. Bird, W. E. Stewart, E. N. Lightfoot, *Transport Phenomena*, John Wiley and Sons, Incorporated, New York, New York, 1960.

[39] J. O. Hirschfelder, C. F. Curtiss, R. B. Bird, *Molecular Theory of Gases and Liquids*, 2nd Edition, John Wiley and Sons, Incorporated, New York, New York, 1964.

[40] S. Takahashi, *Journal of Chemical Engineering of Japan* 7 (6) (1974) 417–420.

[41] B.F. McCoy, H.T. Davis, *Phys. Rev.* A20 (1978) 1201.

[42] C. Miqueu, B. Mendiboure, J. Lachaise, *Ind. Eng. Chem. Res.* 44 (2005) 3321–3329.

[43] H. Lin, Y.-Y. Duan, Q. Min, *Fluid Phase Equil.* 254 (2007) 75–90.

[44] L.M. Pickett, J. Manin, C.L. Genzale, D.L. Siebers, M.P.B. Musculus, C.A. Idicheria, *SAE Int. J. Engines* 4 (2011) 764–799.

[45] L.M. Pickett, C.L. Genzale, G. Bruneaux, L.-M. Malbec, L. Hermant, C. Christiansen, J. Schramm, *SAE Int. J. Engines* 3 (2010) 156–181.

[46] G.A. Bird, *Molecular Gas Dynamics and the Direct Simulation of Gas Flows*, Oxford University Press, 1994.

[47] S.E. Feller, R.W. Pastor, *J. Chem. Phys.* 111 (1999) 1281–1287.

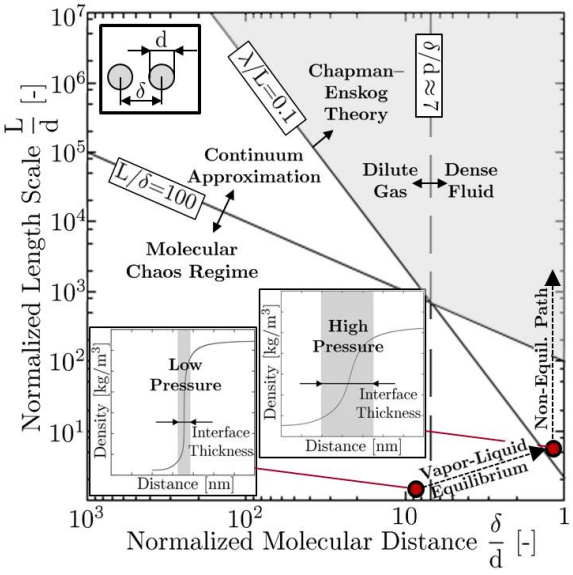

Figure 1: Location of low-pressure and high-pressure gas-liquid interfaces (inset plots) within the regime diagram of microscale flows according to Bird [46]. The highlighted area represents the regime where the Navier-Stokes equations are valid.

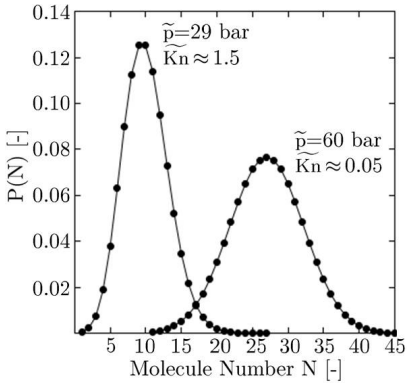

Figure 2: Probability density distributions of a low-pressure and high-pressure interface. The low-pressure interface has a lower value of the average molecule number (nV=10) and a higher coefficient of variation ($c_v \approx 0.32$) in comparison to the high-pressure interface (nV=27, $c_v \approx 0.19$). The lines are for guidance only.

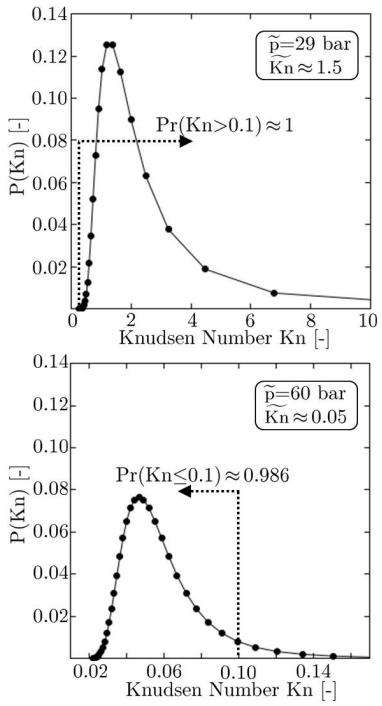

Figure 3: Probability density distributions of the (top) low-pressure and (bottom) high-pressure interfacial Knudsen numbers. Both interfaces are almost certainly governed by (top) classical two-phase theory and (bottom) dense-fluid mixing dynamics. The lines are for guidance only.

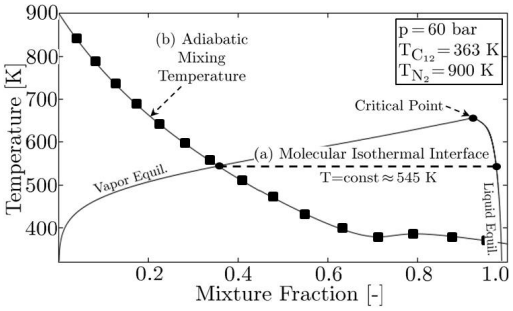

Figure 4: Definition of temperature-mixture composition distributions across (a) a molecular isothermal interface and across (b) an adiabatic interface.

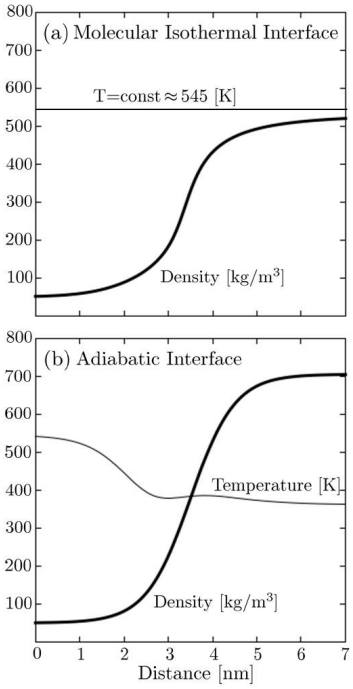

Figure 5: Density and temperature profiles of (top) a molecular interface and (bottom) an adiabatic interface. The adiabatic interface shows an increase in the density gradient and in liquid density along with a more complex temperature distribution in comparison to the molecular interface.

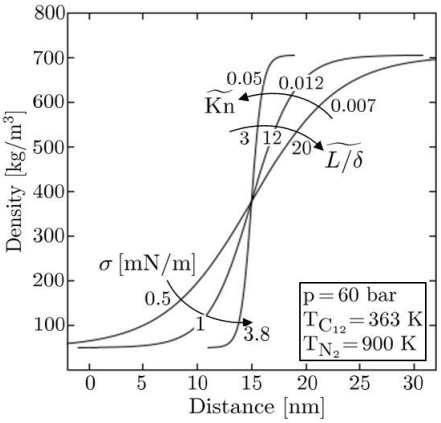

Figure 6: Density profiles along with corresponding mean Knudsen numbers and sample sizes of a disintegrating gas-liquid interface. Respective interfacial free energy forces σ have been obtained from non-equilibrium mean-field thermodynamics according to Eq. (3). The density profile in Fig. 5 (bottom) provides the required modeling closure for Eq. (3). This non-equilibrium pathway of the interface is highlighted in the regime diagram in Fig. 1.

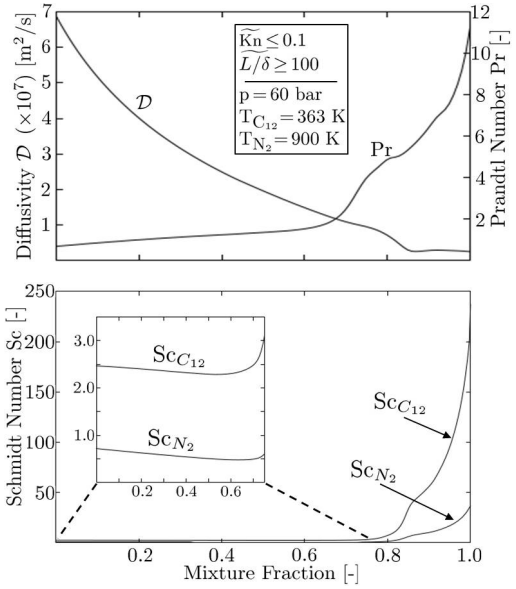

Figure 7: Mixture-composition distributions of (top) diffusivities and Prandtl numbers and (bottom) species-specific Schmidt numbers across an adiabatic and continuous gas-liquid mixing layer.

List of Figures